CFD Letters

Journal homepage:
https://semarakilmu.com.my/journals/index.php/CFD_Letters/index
ISSN: 2180-1363

The impact of mechanical ventilation on Sfax City's greenhouse microclimate

Hamza Chiboub[1], Hasna Abid[1,*], Mariem Lajnef[1], Slim Zouari[2], Giovanni Gugliuzza[3], Maroua Mejri[2], Emilia Arrabito[4], Zied Driss[1]

[1] Laboratory of Electromechanical Systems, National Engineering School of Sfax, University of Sfax, P.O. Box 1173, Road Soukra, 3038 Sfax, Tunisia
[2] Rue de l'Assistance, perpendiculaire à l'avenue Alain Savary – 1003 – Cité El Khadhra, Tunisia
[3] Research Centre for Agriculture and Environment (CREA-AA), Italy
[4] Moncada Soc. Agr. Coop O.P. Address: C.da Scavuzzo snc 97014 Ispica (RG), Italy

ARTICLE INFO

Article history:
Received 22 October 2023
Received in revised 21 November 2023
Accepted 20 December 2023
Available online 31 March 2024

Keywords:
Greenhouse; Crop; Sfax city; Climate; CFD; mechanical ventilation

ABSTRACT

The greenhouse serves as an enclosed structure designed to create a conducive environment for agricultural productivity, irrespective of the challenges posed by seasonal variations. Recognizing the contemporary complexities in agricultural management, our research endeavors involve the development of a comprehensive numerical model and the establishment of an experimental setup to delve into the nuanced impact of mechanical ventilation. Specifically, the study investigates the influence of four different entrance velocity values on airflow dynamics within agricultural greenhouses. The results illuminate the direct correlation between inlet velocity and various crucial variables, including temperature distribution, velocity field distribution, DO irradiation distribution, and static pressure distribution. Notably, at V_{int} = 12 m.s^{-1}, the maximum temperature remains below T_{max} = 307 K, while at V_{int} = 3 m.s^{-1}, it reaches T_{max} = 327 K. This underscores the pivotal role of accurate modeling and control for the optimal management of agriculture in the central region of Tunisia, particularly in Sfax.

1. Introduction

Greenhouses emerge as a solution to maintain consistent agricultural productivity throughout the year by controlling microclimates for various crops. However, the looming threat of acute water scarcity by 2030, a consequence of climate change, is a cause for concern. Greenhouses offer potential water-saving solutions for water-stressed regions [1-3]. The internal conditions of solar greenhouses are influenced by external factors, construction materials, and cultivation practices, which have a direct impact on plant growth dynamics. Temperature and airflow velocity within the greenhouse are critical determinants. Research in this field includes two approaches: experimental and numerical studies, each with its advantages and limitations, contributing to our understanding of solar greenhouse dynamics [4-6].

* *Corresponding author.*
E-mail address: abidhasna@ymail.com (Hasna Abid)

https://doi.org/10.37934/cfdl.16.8.150162

Through the numerical way, Johnston *et al.,* [7] investigated the impact of lowering the height of the greenhouse and introducing covers on its previously open sides within a two-span greenhouse. Their aim was to gain a deeper understanding of how these modifications affect airflow patterns, which could potentially lead to energy conservation. In their 2023 study, Zhang *et al.,* [8] conducted an extensive experimental examination with the specific goal of analyzing the effects of shaded areas within a traditionally designed solar greenhouse, especially regarding their impact on winter tomato growth. El Alaoui *et al.,* [9] utilized CFD techniques to assess the effects of seasonal variations in Morocco, specifically focusing on the periods of October and March. Their method resulted in the development of a "combined data" model, which was created by synthesizing experimental data collected across both months. This model underwent thorough testing and ultimately confirmed its effectiveness in accurately forecasting the internal temperature (Tin) and relative humidity (Rh_{in}) for both March and October, simultaneously. In 2022, Xu *et al.,* [10] created a CFD model to analyze temperature distribution within a greenhouse situated in China. Their study encompassed scenarios with and without the presence of crops. The results uncovered a substantial influence of crops on the temperature distribution inside the greenhouse. This underscores the critical importance of considering the dynamics of plant growth when designing and operating greenhouses.

Furthermore, in the same year, Bekraoui *et al.,* [11] developed a CFD model to scrutinize the microclimate of a tunnel greenhouse dedicated to young citrus saplings. They investigated how this microclimate affected various plant activity parameters, including leaf temperature and transpiration. The findings revealed significant variability in both air and leaf temperatures within the greenhouse, ranging from 6 °C to 33 °C and 8 °C to 30 °C, respectively. Additionally, the research indicated that the indoor air humidity in the greenhouse is exceptionally high, exceeding 80%. Ayed *et al.,* [12] conducted an experimental investigation with the goal of improving greenhouse microclimates by incorporating textile waste into cement blocks. Their findings demonstrated the effectiveness of a hydroponic greenhouse constructed using textile-reinforced cement blocks, which displayed superior thermal efficiency compared to a greenhouse made from Plexiglas. In the same framework, Ben Ali *et al.,* [13] embarked on an experimental study, coupled with MATLAB simulations, to explore the potential of harnessing wind energy for regulating an Insulated Greenhouse (IG) and reducing energy consumption. Their results revealed that the proposed Wind Turbine System (WTS) efficiently met all the power requirements, achieving a Renewable Factor (RF) of 99.96% and a minimal Loss of Power Supply Probability (LPSP) of 0.03.

Examination of the literature reveals a notable absence of discussions on the connection between inlet velocity and indoor airflow characteristics within greenhouses. Consequently, the principal objective of this paper is to fill this knowledge gap by establishing and presenting relationships between inlet velocity and various airflow characteristics. In this study, our primary focus lies within the domain of mechanical ventilation. We engage in a comparative analysis to investigate how four distinct inlet velocities affect airflow characteristics. This analysis is undertaken to clarify the direct relationship between inlet velocity and the resulting airflow characteristics.

2. Methodology

2.1 Experimental Setup

In June 2022, an experimental study was conducted in a polyethylene film greenhouse with a gable roof design in Sfax City, Tunisia, to ensure the reproducibility of a Computational Fluid Dynamics (CFD) simulation and validate its precision. The greenhouse was equipped with mechanical ventilation as depicted in Figure 1, and various sensors were strategically placed inside and outside to monitor environmental conditions. These sensors included a solar radiation sensor, an air

temperature and humidity sensor, and an air velocity sensor. To measure air temperature, ten DHT22 sensors were placed at 20 cm intervals within the greenhouse. Air velocity was measured using a UT363 mini anemometer. Solar radiation was quantified using a solarimeter placed outdoors, carefully positioned to receive direct sunlight and avoid shadows and reflections. This experimental setup was designed to validate the CFD simulation results and allow for detailed comparisons.

Fig. 1. Prototype of an experimental greenhouse

2.2 The Governing Equations

The simulation of the greenhouse in ANSYS Fluent 17.0 employs the three-dimensional (3D) Reynolds-Averaged Navier-Stokes (RANS) model equations to mathematically characterize fluid flow behavior. These equations are grounded in the conservation laws for mass, momentum, and energy. Comprising three integral components: the continuity equation, momentum equations, and energy equation. The RANS equations respectively encapsulate the conservation of mass, the transfer of momentum, and the conservation of energy within the fluid. Additionally, the simulation incorporates the k-ε turbulence model to replicate turbulent flow within the greenhouse. This model addresses two transport equations, one for turbulent kinetic energy (k) and another for its dissipation rate (ε), assuming the definition of turbulent viscosity (μ_t) as outlined by previous research [14-16].

$$\mu_t = \rho C_\mu \frac{k^2}{\varepsilon} \tag{1}$$

In the presented equations, ρ represents the fluid density, and C_μ is a constant. The integration of the Reynolds-Averaged Navier-Stokes (RANS) equations with the k-ε turbulence model facilitates a precise simulation of fluid flow and temperature distributions within the greenhouse. The continuity equation is expressed as follows:

$$\frac{\partial \rho}{\partial t} + \nabla . \left(\rho \vec{V}\right) = 0 \tag{2}$$

In the provided context, "V" represents the mean velocity vector, and ρ denotes the average value of the density.

$$\frac{\partial\left(\rho\vec{V}\right)}{\partial t}+\nabla.\left(\rho\vec{V}\otimes\vec{V}\right)=\nabla.\left(-p\delta+\bar{\bar{\tau}}-\rho\overrightarrow{V'}\otimes\overrightarrow{V'}\right)+S_M \quad (3)$$

The momentum equation is expressed as follows:

In the provided equations, p represents static pressure, t stands for time, $\bar{\bar{\tau}}$ denotes the molecular stress tensor, and δ represents the Kronecker delta function. The terms $\vec{V}'$ and $-\rho\overrightarrow{V'}\otimes\overrightarrow{V'}$ correspond to the fluctuating velocity vector and the Reynolds stress tensor, respectively. Furthermore, SM represents a source term that encompasses centrifugal and Coriolis forces.

The energy equation, expressed in terms of total energy, is presented as follows [17]:

$$\frac{\partial}{\partial t}(\rho E)+\nabla.\left(\vec{V}(\rho E+p)\right)=\nabla.\left(k_{eff}\nabla T\right)+\nabla.\left(\bar{\bar{\tau}}.\vec{V}\right)+S_E \quad (4)$$

In the provided equation, E represents the total energy, T is the static temperature, k_{eff} signifies the effective thermal conductivity, and S_E is a source term. The total energy E is defined as follows:

$$E=e+\frac{\vec{V}^2}{2} \quad (5)$$

In the given context, "e" denotes the static energy.

The discrete ordinate model (DO) has been chosen to calculate radiant solar energy on the walls. For the absorber surface, a fully opaque radiation boundary with an emissivity of 1 and null diffusivity was specified, while a semi-transparent boundary with an emissivity of 0.94 was set for the glass cover boundary. The remaining walls were treated as adiabatic. The DO radiation model solves the radiative transfer equation for a finite number of discrete solid angles, each associated with a vector direction fixed in the global Cartesian system. The DO model addresses the radiative transfer equation in the direction of $\vec{s}$ as presented:

$$\nabla.\left(I_\lambda(\vec{r},\vec{s})\vec{s}\right)+(a_\lambda+\sigma_s)I_\lambda(\vec{r},\vec{s})=a_\lambda n^2 I_{b\lambda}+\frac{\sigma_s}{4\pi}\int_0^{4\pi}I_\lambda(\vec{r},\vec{s}')\,\Phi(\vec{s}.\vec{s}')\,d\Omega \quad (6)$$

In the provided equation, I_λ represents the radiation intensity of wavelength λ, dependent on the position vector $\vec{r}$ and the direction vector $\vec{s}$. Additionally, $I_{b\lambda}$ stands for the black body intensity as determined by the Planck function, a_λ is the absorption coefficient, σ_s represents the scattering coefficient, $\vec{s}'$ is the scattering direction vector, Φ is the phase function, and Ω denotes the solid angle.

2.3 Geometry Configuration and Boundary Conditions

Figure 2 provides an illustration of the computational domain representing the greenhouse being studied. The greenhouse has dimensions of 4 m in length and 2.6 m in width. The crops within the greenhouse are of a size measuring 0.5 m by 0.5 m by 3.5 m. The inlet opening is 0.3 m by 0.3 m, and

the outlet measures 0.5 m by 0.5 m. This paper delves into a comprehensive examination of localized airflow patterns within agricultural greenhouses. This investigation is conducted at four different inlet velocities, aiming to provide a thorough understanding of their effects. Various boundary conditions were implemented, as illustrated in Figure 2, incorporating inlet velocities of V=3 $m.s^{-1}$, V=6 $m.s^{-1}$, V=9 $m.s^{-1}$, and V=12 $m.s^{-1}$. The outlet section was characterized by a fixed zero-gauge pressure. Additionally, the outdoor temperature was set at T_{out}=311 K, and the solar radiation level (R) was maintained at 900 $W.m^{-2}$ based on experimental measurements.

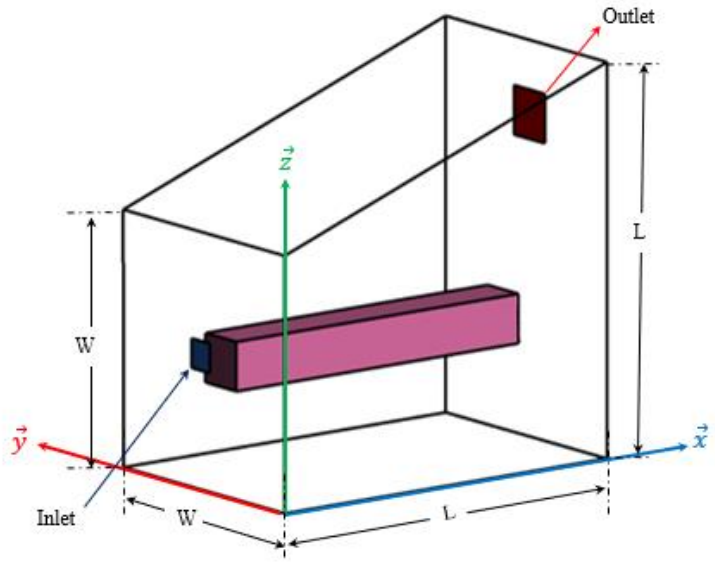

Fig. 2. Computational domain and boundary conditions

2.4 Grid Independency Test and Simulation Setup

Within this section, we delineated four optimized grids employing node counts of 26150, 32474, 46887, and 51428. Figure 3 visually presents temperature values at a designated point with coordinates x = 2 m, y = 1.3 m, and z = 1.7 m across these diverse meshes. Analysis of the figure reveals that meshes 3 and 4 consistently align with experimental data. Consequently, the grid with 46,887 nodes emerged as the preferred choice, striking a balance between validation accuracy and a reasonable resolution time. Hence, Figure 4 presents the created meshing grid consisting of 46887 nodes. Special attention is paid to solver settings and boundary conditions for precision and reliability. The Boussinesq approximation is employed to model air properties [17, 18], particularly accounting for temperature-induced changes in air density due to buoyancy. Turbulence generated by buoyancy forces is described using the RNG k-ε turbulence model. Additionally, the discrete ordinate model (DO) is used to compute solar radiation on the greenhouse walls, considering specific parameters. Various inlet velocities are tested, and a fixed zero-gauge pressure is set at the outlet for results convergence. The SIMPLEC solver algorithm is selected to expedite convergence, and a second-order upwind scheme is used for enhanced accuracy, complemented by default sub-relaxation factors for pressure, density, momentum, and k-ε considerations.

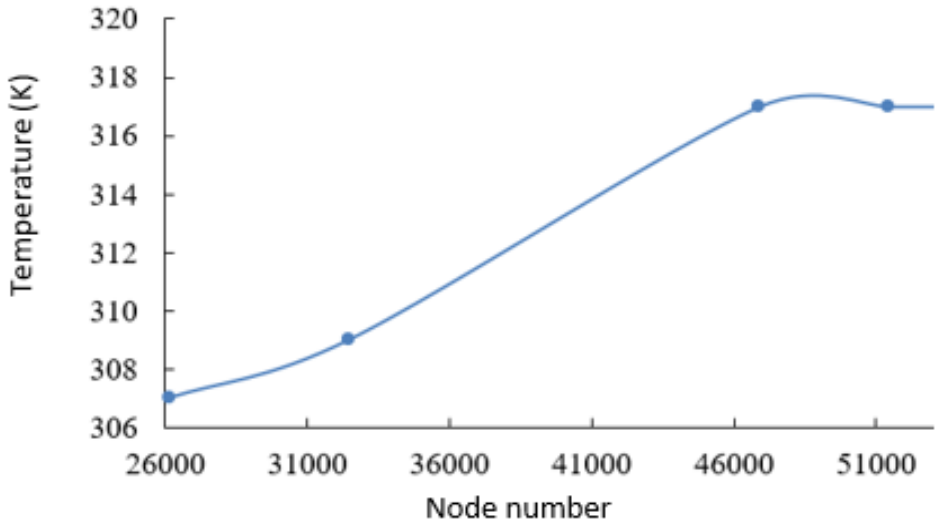

Fig. 3. Temperature sensitivity to the node number at the point characterized by x = 2 m, y = 1.3 m, and z = 1.7 m

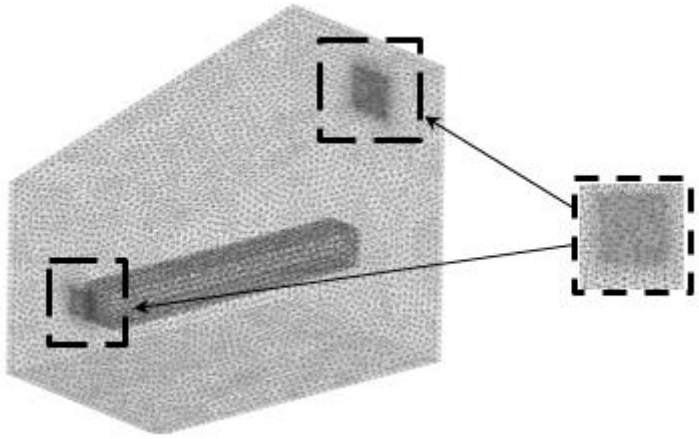

Fig. 4. Computational domain meshing

2.5 Validation using the Experimental Findings

The validation of computational results for the greenhouse scenario with an entrance velocity of V=3 $m.s^{-1}$ was conducted using experimental data collected on June 23, 2022, at 13:00. This procedure confirms the accuracy of the numerical simulation. In Figure 5, a comparison of the computational and experimental air temperature profiles is presented along the visualization line defined by x=2 m and y=1.3 m. These findings reveal a remarkable alignment in behavior between the numerical models and the actual experimental results. Notably, the simulated air temperature profiles faithfully reproduce the patterns observed in the experimental data. The primary distinction between the numerical and experimental results in these conditions is a marginal difference of approximately 5%. The numerical model's predictions' reliability are demonstrated by this very small difference.

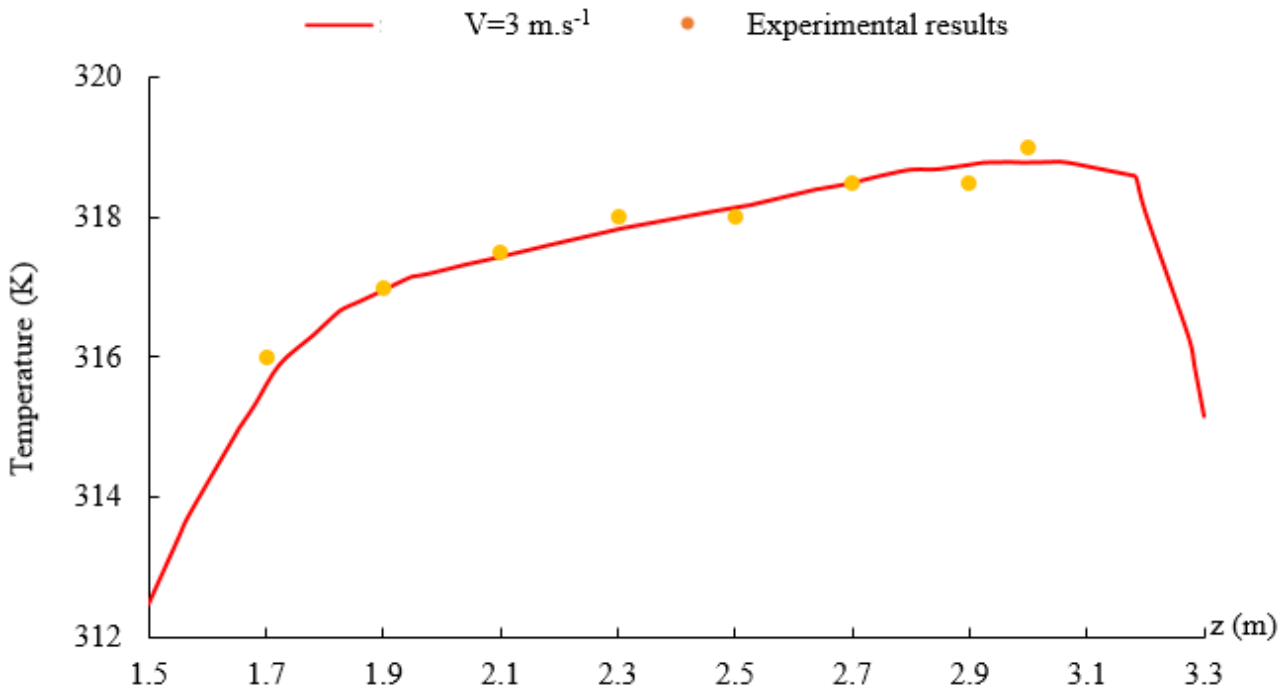

Fig. 5. Simulated and measured temperature at visualization line defined by x=2m and y=1.3m

3. Local Characteristics

The purpose of this section is to offer a comprehensive insight into the aerodynamic characteristics that govern the airflow dynamics within the greenhouse environment. This is achieved by presenting visual maps illustrating the temperature distribution, velocity field, DO irradiation, and static pressure. These visual representations encompass various inlet velocities, specifically V=3 m.s^{-1}, V=6 m.s^{-1}, V=9 m.s^{-1}, and V=12 m.s^{-1}, and are focused on the plane defined by y=1.3 m.

3.1 Temperature Distribution

Figure 6 displays temperature distribution for various inlet velocities. The initial inlet temperature, which is a boundary condition, influences the path of the air as it flows through the crop area. As the air circulates around the crops, its temperature gradually rises. This temperature increase leads to the formation of a thermal plume above the crop area, clear as a rise in air temperature. Additionally, the heated air rises higher due to the buoyancy principle, with the highest corner of the greenhouse experiencing the maximum temperature. The movement of heat, moisture, and gases emitted from the crop surfaces is significantly aided by the presence of this thermal plume, directly impacting the overall temperature distribution within the greenhouse. The thermal effects also cause the greenhouse walls to experience elevated temperatures. Importantly, it's crucial to acknowledge that the internal temperatures of the greenhouse are impacted by the inflow velocity. Higher inlet velocities lead to lower temperature readings. For instance, with V=12 m.s^{-1}, temperature measurements remain within the range of 307 K. However, for V=3 m.s^{-1}, they reach T=327 K, which is the upper limit. Table 1 presents the summary table of the maximum temperature values for various inlet velocities. Hence, this section underscores the importance of airflow control and ventilation systems to maintain optimal crop conditions and overall greenhouse performance.

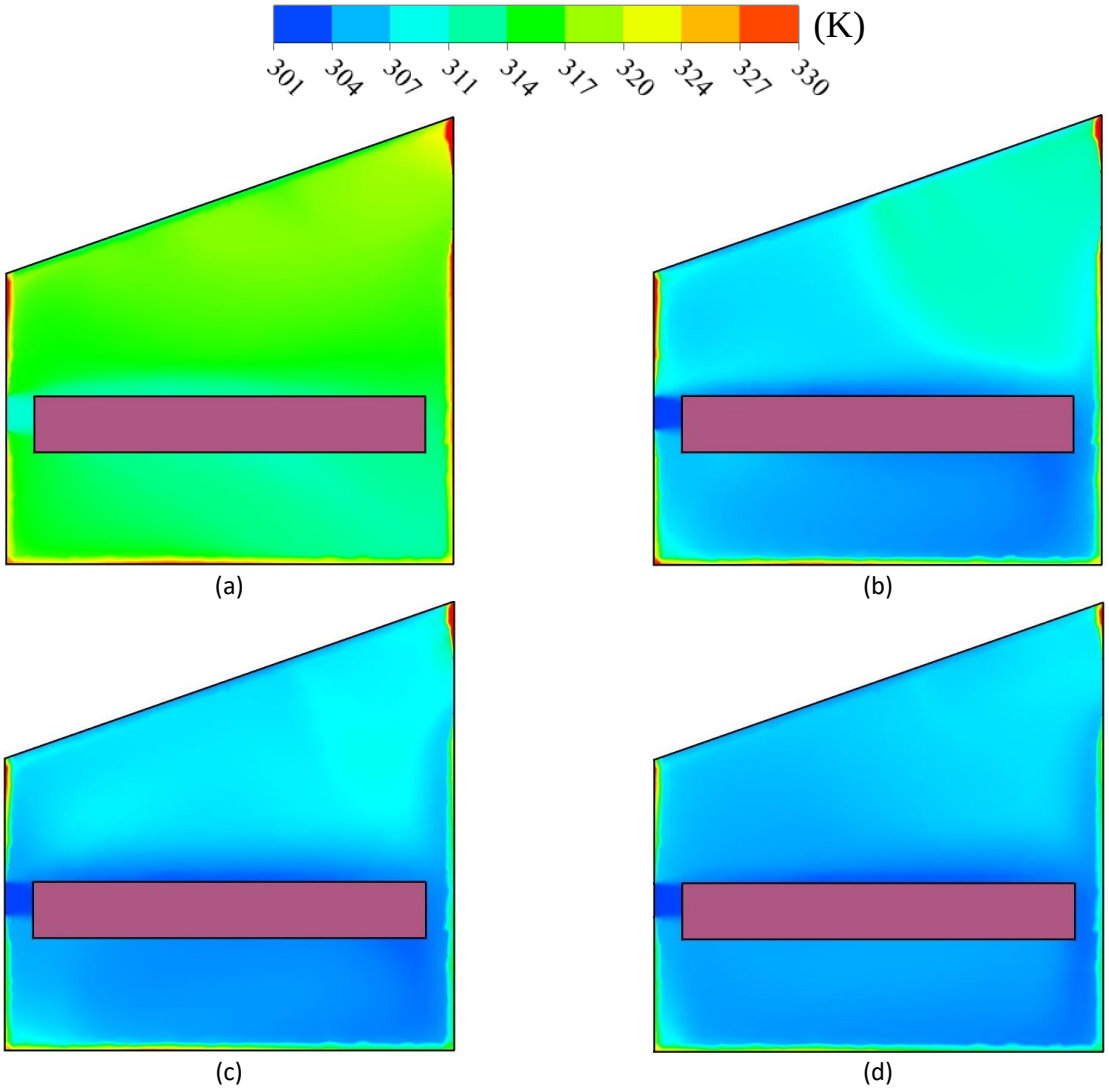

Fig. 6. Temperature distribution in the cross plan: (a) V=3m.s^{-1}, (b) V=6m.s^{-1}, (c) V=9m.s^{-1} and (d) at V=12m.s^{-1}

Table 1
Presentation of the maximum temperature values for various inlet velocities

	V_{int}=3 m.s^{-1}	V_{int}=6 m.s^{-1}	V_{int}=9 m.s^{-1}	V_{int}=12 m.s^{-1}
T_{max}	327 K	319 K	312 K	307 K

3.2 Velocity Fields Distribution

Figure 7 displays velocity field maps within the greenhouse. At the entrance inlet, a distinctive discharge zone forms, which interacts with the adjacent cropland. Above the crops, a heat plume develops, leading to a limited increase in velocity. Importantly, there is a direct correlation between the inlet velocity and the extent of this velocity increase. As the airflow progresses through the greenhouse, its velocity gradually decreases, reaching its lowest point as it exits through the outlet. The figure reveals the presence of multiple recirculation zones scattered throughout the greenhouse area, and these zones are highly dependent on the chosen inlet velocity. These circulation zones contribute significantly to the creation of a more consistent microclimate. This uniformity has the potential to have a significant impact on crop development, eventually improving yield quality.

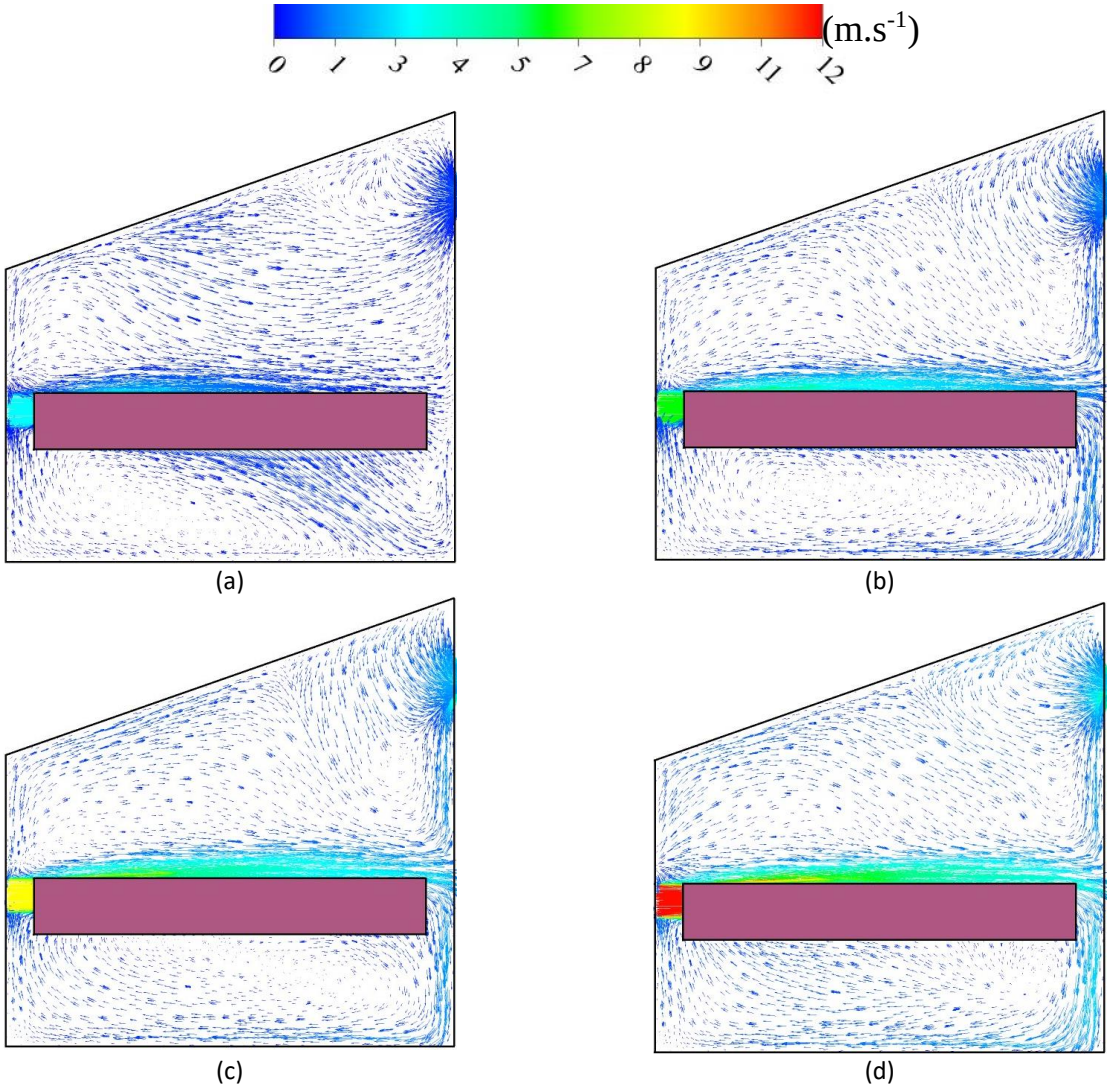

Fig. 7. Velocity field maps in the cross plan: (a) V=3m.s^{-1}, (b) V=6m.s^{-1}, (c) V=9m.s^{-1} and (d) at V=12m.s^{-1}

3.3 DO Irradiation Distribution

Detailed DO irradiation distribution within the greenhouse can be found in Figure 8. This variable plays a pivotal role in shaping the microclimate within the greenhouse and influencing the growth of its crops. It quantifies the percentage of diffuse solar radiation inside the greenhouse concerning the total solar radiation. Near the entrance of the greenhouse, the DO irradiation starts at a relatively low value. However, it gradually increases as solar radiation penetrates the greenhouse space, reaching its peak at the top of the greenhouse structure. Notably, the highest DO irradiation coincides with V=3 m.s^{-1}, indicating the most favorable light dispersion throughout the greenhouse. Table 2 presents the summary table of the maximum DO irradiation values for various inlet velocities. This finding emphasizes the interdependence between the selected inlet velocity and the amount of DO radiation, which influences the greenhouse's bright environment.

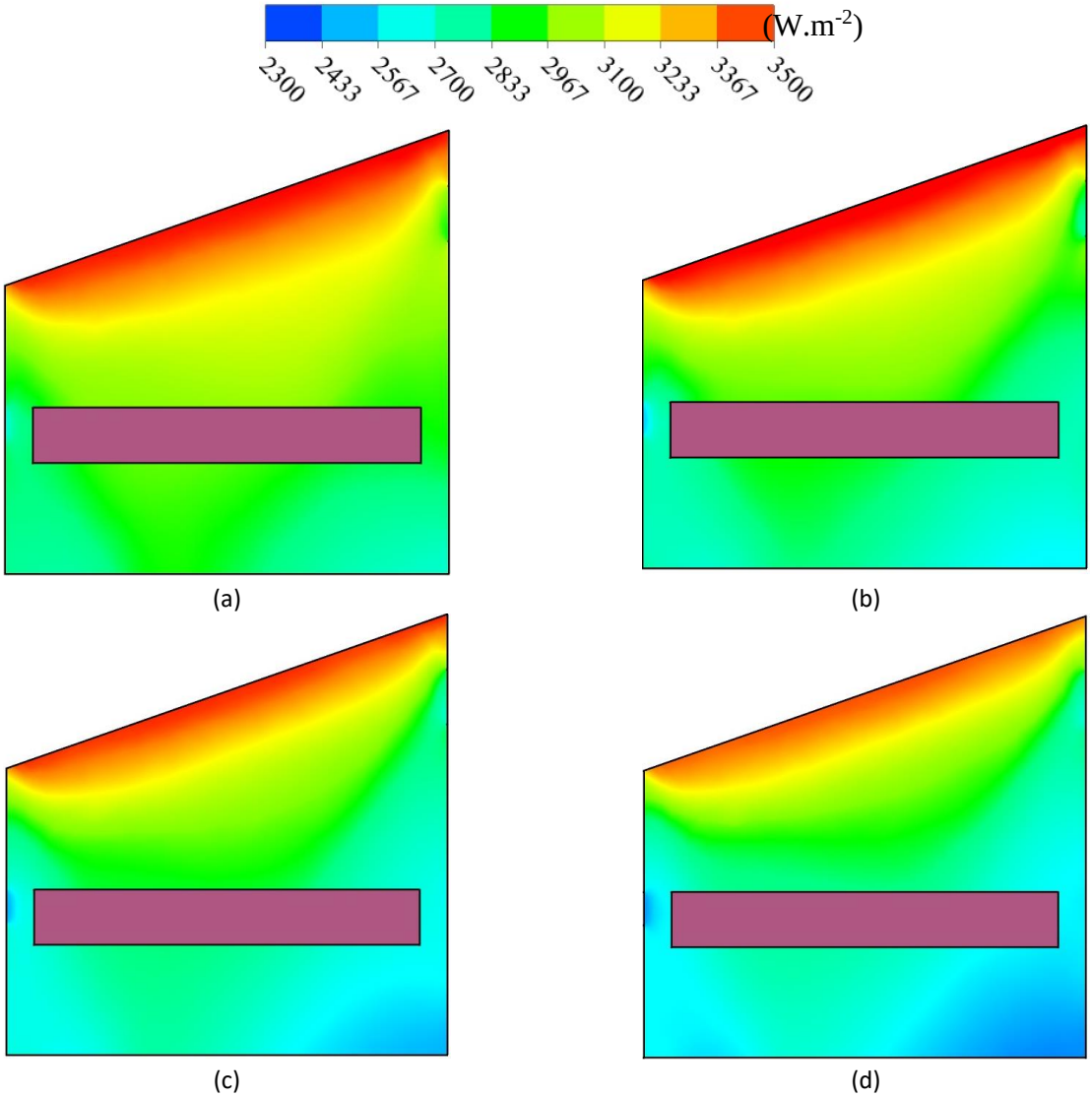

Fig. 8. DO irradiation distribution in the cross plan: (a) V=3m.s^{-1}, (b) V=6m.s^{-1}, (c) V=9m.s^{-1} and (d) at V=12m.s^{1}

Table 2
Presentation of the maximum DO irradiation values for various inlet velocities

	V_{int}=3 m.s^{-1}	V_{int}=6 m.s^{-1}	V_{int}=9 m.s^{-1}	V_{int}=12 m.s^{-1}
DO_{max}	3548 W.m^{-2}	3527 W.m^{-2}	3478 W.m^{-2}	3429 W.m^{-2}

3.4 Static Pressure Distribution

The static pressure distribution within the greenhouse is depicted in Figure 9. In the lower part of the greenhouse, beneath the plant canopy, a noticeable area of decreased pressure emerges, characterized by the lowest static pressure value. This value varies depending on the inlet velocity, increasing from 5 Pa at an inlet velocity of 3 m.s^{-1} to 18 Pa at an inlet velocity of 12 m.s^{-1}. The airflow decelerates in this zone due to obstructions like the crop canopy, resulting in a minor decrease in air pressure. At the upper boundary of the greenhouse, a distinct compression zone becomes apparent, where static pressure reaches its maximum, as the airflow ascends through the greenhouse. In this area, as the airflow accelerates, reduced resistance results in a slight increase in air pressure. Interestingly, the static pressure clearly decreases at the outlet level. It's worth noting that the

highest value within the compression zone aligns with an inlet velocity of V=12 m.s^{-1}, underscoring the significant influence of inlet velocity on this phenomenon. Table 3 presents the summary table of the of the maximum static pressure values for various inlet velocities. This discovery highlights the connection between input velocity and the behavior of the compression zone.

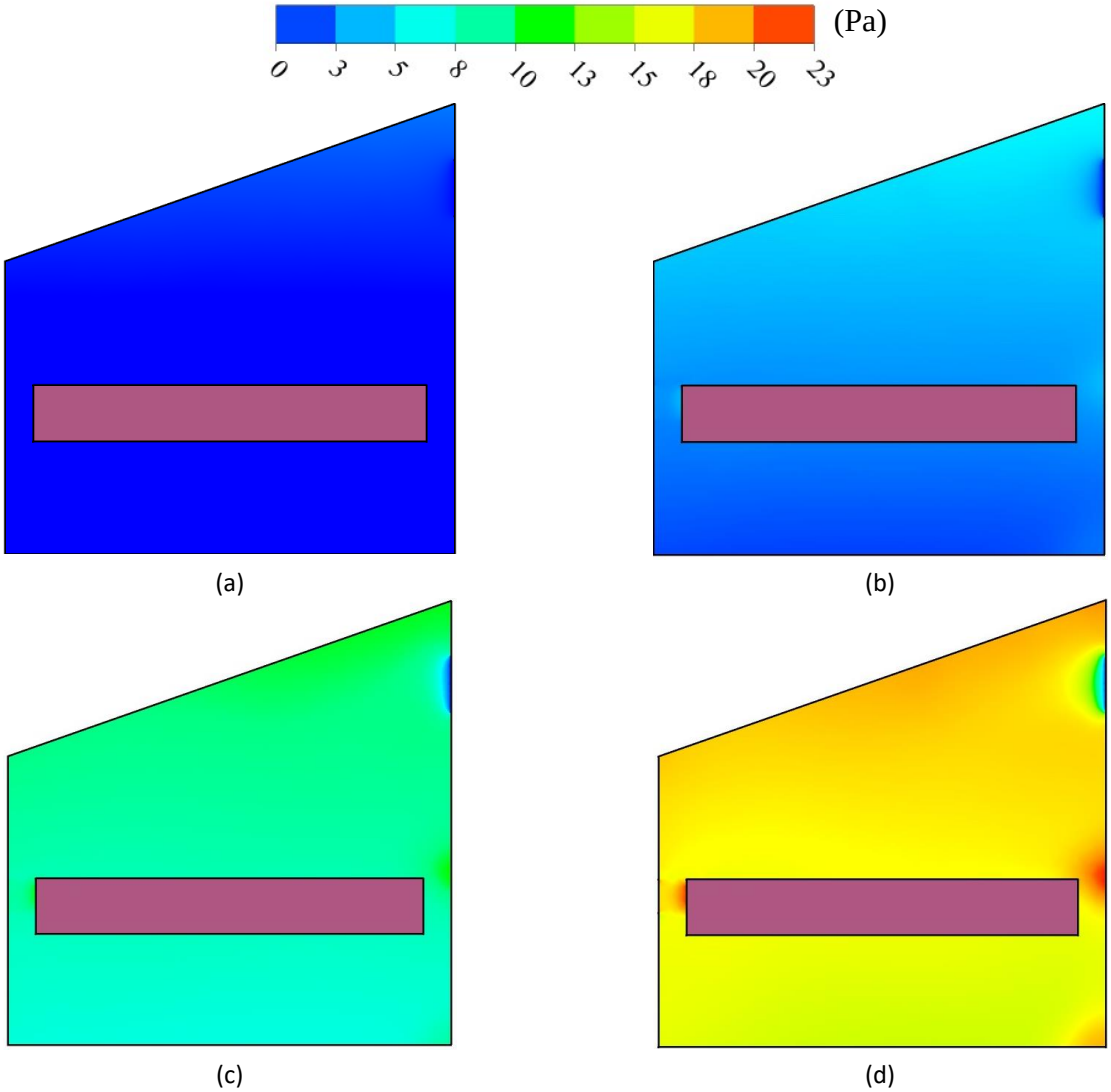

Fig. 9. Static pressure maps in the cross plan: (a) V=3m.s^{-1}, (b) V=6m.s^{-1}, (c) V=9m.s^{-1} and (d) at V=12m.s^{-1}

Table 3
Presentation of the static pressure values for various inlet velocities

	V_{int}=3 m.s^{-1}	V_{int}=6 m.s^{-1}	V_{int}=9 m.s^{-1}	V_{int}=12 m.s^{-1}
P_{max}	2.1 Pa	5.6 Pa	11.6 Pa	22.6 Pa

4. Conclusion

This study explores the impact of mechanical ventilation on airflow characteristics within an agricultural greenhouse. The investigation utilizes both experimental set up and a comprehensive Computational Fluid Dynamics (CFD) model to assess the influence of air, crops, and soil, with a focus on accuracy verification. The CFD model's outcomes are subsequently validated by comparing them with data obtained from an experimental greenhouse prototype situated in Sfax.

i. The inlet velocity has a noticeable effect on temperature distribution. With an inlet velocity of V=12 $m.s^{-1}$, temperature measurements stay within the range of 307 K, whereas they exceed 327 K for V=3 $m.s^{-1}$.
ii. In addition to temperature, the intake velocity significantly influences the velocity field distribution within the greenhouse.
iii. The inlet velocity also has a substantial impact on the distribution of DO irradiation. Notably, the maximum DO irradiation is observed at an inlet velocity of V=3 $m.s^{-1}$, indicating optimal light dispersion throughout the greenhouse.
iv. The inlet velocity directly affects the distribution of static pressure. The highest value within the compression zone corresponds to an inlet velocity of V=12 $m.s^{-1}$.

Acknowledgement
The author(s) received financial support for the research from the Tunisian Italian program INTESA https://www.italietunisie.eu/projets/les-projets/intesa/

References

[1] Ghoulem, Marouen, Khaled El Moueddeb, Ezzedine Nehdi, Rabah Boukhanouf, and John Kaiser Calautit. "Greenhouse design and cooling technologies for sustainable food cultivation in hot climates: Review of current practice and future status." *Biosystems Engineering* 183 (2019): 121-150. https://doi.org/10.1016/j.biosystemseng.2019.04.016
[2] Roslan, N., M. E. Ya'acob, M. A. M. Radzi, Y. Hashimoto, D. Jamaludin, and G. Chen. "Dye Sensitized Solar Cell (DSSC) greenhouse shading: New insights for solar radiation manipulation." *Renewable and Sustainable Energy Reviews* 92 (2018): 171-186. https://doi.org/10.1016/j.rser.2018.04.095
[3] Yano, Akira, and Marco Cossu. "Energy sustainable greenhouse crop cultivation using photovoltaic technologies." *Renewable and Sustainable Energy Reviews* 109 (2019): 116-137. https://doi.org/10.1016/j.rser.2019.04.026
[4] Abid, Hasna, Ahmed Ketata, Mariem Lajnef, Hamza Chiboub, and Zied Driss. "Numerical investigation of greenhouse climate considering external environmental factors and crop position in Sfax central region of Tunisia." *Solar Energy* 264 (2023): 112032. https://doi.org/10.1016/j.solener.2023.112032
[5] Abid, Hasna, Ismail Baklouti, Zied Driss, and Jamel Bessrour. "Experimental and numerical investigation of the Reynolds number effect on indoor airflow characteristics." *Advances in Building Energy Research* 14, no. 4 (2020): 424-449. https://doi.org/10.1080/17512549.2019.1660711
[6] Abid, Hasna, and Zied Driss. "Computational study and experimental validation on the effect of inlet hole surface on airflow characteristics and thermal comfort in a box occupied by a thermal manikin." *International Journal of Ventilation* 21, no. 2 (2022): 140-156. https://doi.org/10.1080/14733315.2020.1812223
[7] Johnston, Larz, Ramadas Narayanan, and Mohan R. Moola. "CFD investigation on key design parameters of a hoop-type greenhouse." (2023).
[8] Zhang, Rui, Yichuan Liu, Delan Zhu, Xiaomin Zhang, Liqiong Lu, Fei Gao, and Changjuan Zheng. "Dynamics of shaded areas in a typical-shaped solar greenhouse and their effects on tomato growth—A case study in winter." *Scientia Horticulturae* 312 (2023): 111882. https://doi.org/10.1016/j.scienta.2023.111882
[9] El Alaoui, Meryem, Laila Ouazzani Chahidi, Mohamed Rougui, Abdellah Mechaqrane, and Senhaji Allal. "Evaluation of CFD and machine learning methods on predicting greenhouse microclimate parameters with the assessment of seasonality impact on machine learning performance." *Scientific African* 19 (2023): e01578. https://doi.org/10.1016/j.sciaf.2023.e01578
[10] Xu, Ke, Xuan Guo, Junming He, Bin Yu, Jinglu Tan, and Ya Guo. "A study on temperature spatial distribution of a greenhouse under solar load with considering crop transpiration and optical effects." *Energy Conversion and Management* 254 (2022): 115277. https://doi.org/10.1016/j.enconman.2022.115277
[11] Bekraoui, Adil, Hicham Fatnassi, Ahmed Mohammed Saad Kheir, Sanae Chakir, Allal Senhaji, Mhamed Mouqallid, and Hassan Majdoubi. "Study of Microclimate and Sapling Citrus Plant Transpiration in Tunnel Greenhouse Under Mediterranean Conditions." *Acta Technologica Agriculturae* 25, no. 2 (2022): 61-66. https://doi.org/10.2478/ata-2022-0010

[12] Ayed, Rabeb, Amira Dellagi, Safa Skouri, Sara Baddadi, Salwa Bouadila, and Mariem Lazaar. "Sustainable insulation solutions for hydroponic greenhouses: The effects of textile waste reinforcement on thermal microclimate." *Journal of Building Engineering* 73 (2023): 106710. https://doi.org/10.1016/j.jobe.2023.106710

[13] Ali, Rim Ben, Salwa Bouadila, Müslüm Arıcı, and Abdelkader Mami. "Feasibility study of wind turbine system integrated with insulated Greenhouse: Case study in Tunisia." *Sustainable Energy Technologies and Assessments* 47 (2021): 101333. https://doi.org/10.1016/j.seta.2021.101333

[14] Kek, Hong Yee, Huiyi Tan, Desmond Daniel Chin Vui Sheng, Yi Lee, Nur Dayana Ismail, Muhd Suhaimi Deris, Haslinda Mohamed Kamar, and Keng Yinn Wong. "A CFD assessment on ventilation strategies in mitigating healthcare-associated infection in single patient ward." *Progress in Energy and Environment* (2023): 35-45. https://doi.org/10.37934/progee.24.1.3545

[15] Tey, Wah Yen, Yutaka Asako, Nor Azwadi Che Sidik, and Rui Zher Goh. "Governing equations in computational fluid dynamics: Derivations and a recent review." *Progress in Energy and Environment* (2017): 1-19.

[16] Elhadad, Alaaeldeen M., and Abo El-Ela. "Experimental and Cfd Resistance Validation of Naval Combatant Dtmb 5415 Model." *Experimental and Cfd Resistance Validation of Naval Combatant Dtmb* 5415.

[17] Al-Rawi, Mohammad, Nived Rajan, Sreeshob Sindhu Anand, Tony Pauly, and Nikhil Thomas. "Prototyping Roof Mounts for Photovoltaic (PV) Panels: Design, Construction and CFD Validation." *CFD Letters* 14, no. 2 (2022): 59-71. https://doi.org/10.37934/cfdl.14.2.5971

[18] Fluent, Ansys. "17.0 Theory Guide. (2016) ANSYS Inc." *Canonsburg, PA, USA*.